Electronic Supplementary Material(ESI) for Nanoscale
This Journal is © The Royal Society of Chemistry 20**

Electronic Supplementary Information

In-situ growth of gold nanoparticles on Hg^{2+}-binding M13 phage for mercury sensing

Xiao-Yan Wang[†], Ting Yang[†], Xiao-Xiao Zhang, Ming-Li Chen, Jian-Hua Wang [*]*

Research Center for Analytical Sciences, Department of Chemistry, College of Sciences, Northeastern University, Box 332, Shenyang 110819, China

E-mail address: yangting@mail.neu.edu.cn, jianhuajrz@mail.neu.edu.cn.

Electronic Supplementary Information Included:

Figure S1. Binding affinity of the selected Hg^{2+}-binding phages for Hg^{2+}.

Figure S2. Binding specificity of the selected Hg^{2+}-binding phages for Hg^{2+}, Cu^{2+} and Cd^{2+}.

Figure S3. λ_{max} for the AuNPs-phage networks with different synthesis conditions of phage concentration (A) and solution acidity (B).

Figure S4. UV-vis absorption spectra of the AuNPs-phage networks before and after the addition of Hg^{2+}. Hg^{2+} concentration: 10 μmol L^{-1}.

Figure S5. Absorbance at λ_{max} for the AuNPs-phage networks as a function of the phage concentration.

Figure S6. XPS spectra of AuNPs in the absence of Hg^{2+} (A); and XPS spectra in the presence of Hg^{2+} (B: 30 μmol L^{-1}; C and D: 50 μmol L^{-1}).

Figure S7. The SPR band (λ_{max}) of AuNPs after the addition of Hg^{2+} of various concentrations.

Figure S8. TEM images of AuNPs before (A) and after the addition of 10 μmol L^{-1} (B) and 200 μmol L^{-1} of Hg^{2+} (C) and the corresponding UV-vis absorption spectra (D).

Figure S9. UV-vis absorption spectra of AuNPs with excessive phages removed upon the addition of Hg^{2+}.

Figure S10. UV-vis absorption spectra of the AuNPs-phage networks upon the addition of Hg^{2+} as a function of time.

Figure S11. UV-vis absorption response to Hg^{2+} of the AuNPs-phage networks prepared with 4 kinds of the selected Hg^{2+}-binding phages.

Figure S12. UV-vis absorption spectra of the AuNPs-phage networks with the addition of different metal cations. Hg^{2+}: 5 μmol L^{-1}, other metal cations: 50 μmol L^{-1}.

1. Experimental details

1.1 Chemicals and materials used in the biopanning process

Unless otherwise specified, all the chemicals used in the present study were analytical reagent grade obtained from the Sinopharm Chemical Reagent Co. (Shanghai, China). Deionized water (DI water, 18.2 MΩ cm, 25℃) was used throughout. Affimag™ γ-Fe_2O_3 (4-5 μm, epoxy content is 200-300 μmol g^{-1} as claimed by the manufacturer) was purchased from Baseline ChromTech Research Centre (Tianjin, China). Horseradish peroxidase-conjugated anti-M13 antibody and 2,2′-azinobis (3-ethylbenthiazoline-6-sulfonic acid) (ABTS) used for ELISA were received from GE healthcare (US) and Sigma-Aldrich, respectively. The centrifugal filter device with MWCO of 100 kDa employed to isolate phages from the eluate was obtained from Millipore (US), and M13 phage DNA extraction kit for phage ssDNA extraction was purchased from BioTeke Co. (Beijing, China).

A phage display peptide library for biopanning of Hg^{2+}-binding phage together with its host cell *E. coli*. ER2738 (Ph.D., Phage Display Peptide Library Kit) was purchased from NEB (New England Bio-Labs, US).LB medium (10 g tryptone, 5 g yeast extract, 5 g NaCl in 1 L DI water, pH 7.0-7.2) with 20 mg L^{-1} tetracycline was used for host cell culture and phage amplification. In order to avoid wild-type phage contamination, all solutions used were sterilized either by autoclave procedure (121℃, 20 min) or passing through 0.22 μm sterilizing filter, and the pipette tips equipped with filter cartridge were used throughout.

1.2 The immobilization of metal cations on magnetic microbeads

2 mL of Affimag™ γ-Fe_2O_3 (1% (w/v)) was incubated in the mixture of 4 mL of $NaHCO_3$-Na_2CO_3 (0.1 mol L^{-1}, pH 9.5) buffer solution and 4 mL of iminodiacetic acid (IDA, 5% (w/w), pH 9.16) for 24 h (37℃, 250 rpm), resulting in IDA functionalized magnetic microbeads, i.e., Affimag™ γ-Fe_2O_3-IDA. It was then rinsed for 3 times with DI water and stored at 4℃in PBS buffer solution (pH 7.4) for future use.

To prepare Hg^{2+}-loaded magnetic microbeads, 500 μL of Affimag™ γ-Fe_2O_3-IDA microbeads (1% (w/v)) was incubated in 5 mL of Hg^{2+} (0.1mol L^{-1}) solution overnight (37℃, 250 rpm), which was then rinsed for 3 times with PBS buffer solution (pH 5.8) and stored in PBS (pH 5.8) at 4℃ for future use. It was labeled as Hg^{2+}-γ-Fe_2O_3. Microbeads loading with other metals were prepared in a similar procedure, except for that the metal salts were replaced by $ZnSO_4 \cdot 7H_2O$, $CdCl_2 \cdot 2.5H_2O$, $Fe(NO_3)_3 \cdot 9H_2O$ and $CuSO_4 \cdot 5H_2O$.

1.3 Screening for Hg^{2+}-binding phage with high selectivity

Negative screening against other metal cations was first conducted to eliminate phages bind with other metal cations. 10 μL of the phage library (~1.8×10^{11}virions, library complexity (unique clones)of ~2.8×10^{9} as claimed by NEB) was dissolved in 500 μL of PBS buffer solution (pH 5.8) and was then mixed with 200 μL of M^{+}-γ-Fe_2O_3 (M^{+} represents Zn^{2+}, Cd^{2+}, Fe^{3+} and Cu^{2+}), followed by shaking for 25 min (100 rpm, 25℃). Thereafter, the supernatant was collected and further amplified.

Considering the phage tittering results (Table S2), negative screening against Zn^{2+}, Cd^{2+}, Fe^{3+} and Cu^{2+} were conducted for 1, 1, 2 and 1 rounds.

Positive screening against Hg^{2+} was afterwards conducted for three rounds to obtain phages with high affinity with Hg^{2+}. 10 μL of the phage solution amplified after the previous step (5.6×10^{11} virions) was dissolved in 500 μL of PBS buffer solution (pH 5.8). It was then mixed with 200 μL of Hg^{2+}-γ-Fe_2O_3. The mixture was allowed to shake for 25 min (100 rpm, 25℃). The supernatant was discarded and the microbeads were washed for twice with PBS buffer solution (pH 5.8) to remove the loosely bonded phages. 1 mL of EDTA solution (0.5 M, pH 8.0) was then added and allowed to shake with the microbeads for 10 min (200 rpm, 25℃). The eluate was further centrifuged with a centrifugal filter device with MWCO of 100 kDa (5000 rpm, 15 min, 4℃) to separate the phages with co-eluted Hg^{2+} ions. Phages retained on the filter membrane were carefully collected, amplified and tittered for conducting the next round of positive screening.

In order to increase the biopanning strength and to get phages with higher affinity to Hg^{2+}, the Hg^{2+} loaded on the microbeads were reduced by eluting with PB buffer solution (pH 3) in the third round of the positive screening.

1.4 Enzyme-linked immunosorbent assay (ELISA) of the selected Hg^{2+}-binding phages

Among the Hg^{2+}-binding phages went through the whole biopanning process, 20 of blue plaques were randomly selected from the final titering plate and the individual phage clones were amplified. The affinity of the selected phages towards Hg^{2+} was

testified using ELISA assay. Briefly, 100 μL of the amplified individual phage clones (2×10^{11} pfu mL^{-1}, diluted with LB medium) was mixed with 200 μL of Hg^{2+}-γ-Fe_2O_3. After incubation at room temperature for 12 h, the microbeads were washed with PBS (pH 5.8) buffer solution for 3 times to remove the loosely bonded phages. 1 mL of horseradish peroxidase (HRP)-conjugated anti-M13 antibody (1:5000 in PBS buffer, pH 5.8) was then added to allow incubation with phages bond to the Hg^{2+}-γ-Fe_2O_3 for 1 h. After washing with PBS buffer (pH 5.8, containing 0.5% Tween 20) for 3 times, 400 μL of a substrate solution (22 mg ABTS in 100 mL PBS (pH 5.8), 30% H_2O_2 with 10^5-fold dilution before use) was added to allow incubation for 1 h. ABTS is oxidized by H_2O_2 under the catalysis of HRP, resulting in a green product with a λ_{max} at 410 nm. The absorbance of the supernatant at 410 nm was recorded with a microplate reader. Among the 20 individual phage clones (P1 to P20) tested, all of the phages showed high affinity for Hg^{2+} except for phage P4 (Figure S1). In order to screen phages with high binding specificity for Hg^{2+}, phage P1, P2, P5, P6, P7, P8, P9, P10, P13, P15, P18 were further conducted with phage ELISA assay against foreign metal ions including Cu^{2+} and Cd^{2+}. As can be seen in Figure S2, phage P1, P2, P8 and P9 possess exclusive affinity for Hg^{2+}, thus were picked and further used for the in situ growth of AuNPs and the ensuing mercury sensing.

1.5 DNA extraction and sequencing

The phages' ss DNA were extracted using M13 phage DNA extraction kit and sequenced by Shanghai Sangon Biotech Co. (Shanghai, China). The corresponding amino sequences of the selected phages were then derived. The sequence of phages

with high specificity for Hg^{2+} (P1, P2, P8 and P9) and phage P6 as the representative of the phages with low specificity were identified and compared in Table S3.

2. Supplemental tables and figures

Table S1. Comparison of the present AuNPs colorimetric sensor with reported AuNPs sensors for colorimetric sensing of Hg^{2+}.

Sensing strategy	AuNPs functionalization	Masking agent	Real sample	LOD (nM)	Ref
Carboxylic group-Hg^{2+} coordination	Carboxylated peptide	Data not shown	None	20,000	[1]
T-Hg^{2+}-T	Poly-T_{33} ssDNA	None	None	250	[2]
Carboxylic group-Hg^{2+} coordination	MPA&AMP	None	None	500	[3]
Hg^{2+}-bis-thymine complex	ssDNA	PDCA	Underground water	10	[4]
T-Hg^{2+}-T	Anti-Hg^{2+} aptamer	None	Tap/lake water	0.6	[5]
Carboxylic group-Hg^{2+} coordination	L-cycteine	None	None	100	[6]
Sulfur-Hg^{2+}-Sulfur	Dithioerythritol	EDTA	None	100	[7]
Hg-Au alloy	Tween 20	EDTA	Sea/drinking water	100	[8]
S-Hg^{2+}-S	Quaternary ammonium group-terminated thiols	None	Drinking water	30	[9]
NTA-Hg^{2+} coordination	3-nitro-1H-1,2,4-triazole	None	Lake water	7	[10]
Riboflavin-Hg^{2+}	Riboflavin	None	Synthetic samples	14	[11]
S-Hg^{2+}-S	Thiol-containing ligand of diethyldithiocarbamate	None	Drinking water	2.9	[12]
T-Hg^{2+}-T	5'-T_{10}-3'	None	River water	17.5	[13]
T-Hg^{2+}-T	ssDNA	None	River/pond water	50	[14]
Bipy-induced aggregation	None	None	River/tap water	38	[15]
S-Hg^{2+}-S	Thiocyanuric acid	None	Lake/tap water	0.5	[16]
T-Hg^{2+}-T	ssDNA	None	None	0.025	[17]
PSS/(T-80)-AuNPs	PSS/T-80	None	None	48.95/255.36	[18]
DNA-AuNPs	DNA	None	None	15	[19]
M13-$Hg^{2+}$and Hg-Au alloy	None	None	River/snow water	80	This work

Table S2. The phage titer results at each stage of the biopanning process.

Biopanning steps		Flowthrough ($\times 10^{10}$pfumL^{-1})	Elute ($\times 10^{7}$ pfumL^{-1})	Amplified for next cycle ($\times 10^{10}$pfumL^{-1})	Recovery (%)
Negative screening	Zn	3.8	—	500	0.150
	Cd	4.3	—	2700	0.611
	Fe_1	0.8	—	1200	0.0136
	Cu	13	—	5600	0.715
	Fe_2	9	—	2800	0.106
Positive screening	Hg_1	—	21	77	0.0009
	Hg_2	—	0.31	276	0.0005
	Hg_3	—	2.56	—	0.0011

For positive screening results, Recovery = output/input = virions of eluate/virions of amplified phage from the last round;

For negative screening results, Recovery = output/input = virions of supernatant/virions of amplified phage from the last round;

Table S3. XPS data for AuNPs before and after the addition of Hg^{2+}.

C(Hg^{2+}) /μM	Name	Peak BE	FWHM /eV	Area (P) CPS. /eV	At./ %
0	Au4f7	83.3	0.52	39110.13	100
30	Au4f7	83.22	0.66	29270.77	94.26
	Hg4f7	99.03	0.55	1964.69	5.74
50	Au4f7	83.7	0.62	5307.3	89.5
	Hg4f7	99.51	0.74	686.12	10.5

Table S4. Comparison of relative response to other metal cations by the AuNPs-phage networks prepared by Hg^{2+}-binding phage and phage library. (Concentration of metal cations is 50 μmol L^{-1} and that of Ag^{+} and Hg^{2+} are 10, 5 μmol L^{-1}, respectively. Data corresponding to Figure 4)

Coexisting ions	**Respond percentage compare to Hg^{2+}/%**	
	Hg^{2+}-binding phage	Phage library
Hg	100.0	100.0
K	6.6	21.7
Na	2.2	13.9
Ca	1.9	21.1
Mg	1.4	11.2
Cd	4.8	13.0
Co	1.0	13.1
Cr	4.0	4.3
Cu	6.4	16.0
Fe	2.1	20.1
Mn	5.0	2.2
Ni	6.0	21.3
Zn	3.8	8.8
Al	4.6	8.4
Ag	6.9	31.4

Table S5. Comparison of tolerance levels of metal cations for the detection of Hg^{2+} between the AuNPs-phage networks and other AuNPs.

Coexisting ions	**Tolerance level /μM**								
	AuNPs-phage network	8-hydroxyquinolines &oxalates-AuNPs	Bismuthiol II - AuNPs	Dithioerythritol - AuNPs	T-Hg^{2+}-T-AuNPs system	Tween 20 -AuNPs	T-Hg^{2+}-T-AuNPs system	MPA&AMP -AuNPs	MPA-AuNPs
K^{+}	100,000	6,000	-	-	-	100	-	-	-
Na^{+}	150,000	6,000	120	-	-	100	-	-	-
Mg^{2+}	30,000	3,000	120	600	-	100	100	1,000	100
Ca^{2+}	1,000	6,000	120	600	-	100	100	1,000	100*
Al^{3+}	30,000	60	120	-	100	100	-	-	100
Fe^{3+}	300	30	120	600	-	100	-	1,000	100
Cu^{2+}	500	-	120	600	100	100	100	1,000	100
Ni^{2+}	1,000	60	120	600	-	100	100	1,000	100
Co^{2+}	500	30	120	600	-	100	100	1,000	100
Mn^{2+}	60	300	120	600	-	100	100	1,000	100*
Cr^{3+-}	6,000	300	4.8	-	-	100	-	1,000	100*
Cd^{2+}	1,000	300	48	600	-	-	100	-	100*
Zn^{2+}	2,000	60	120	600	-	100	100	-	100
Ref	This study	[20]	[21]	[7]	[5]	[8]	[22]	[3]	[23]

*with masking agent 2, 6-Pyridinedicarboxylic acid (PDCA) added.

Table S6. Recovery analysis of the determination of mercury ions in snow and river water as the real samples.

Sample	Added(μM)	Found(μM)	Recovery(%)	RSD%(n=3)
Snow water	2.0	2.46	123.0	4.9
	3.0	2.90	96.5	4.4
	4.0	3.51	87.8	3.6
	5.0	4.55	91.1	7.7
	6.0	6.01	100.2	10.5
	7.0	7.47	106.7	1.5
River water	1.0	1.07	107.0	0.9
	2.0	1.89	94.6	6.3
	3.0	2.87	95.8	8.9
	4.0	4.24	106.0	3.4
	5.0	5.48	110.0	0.4
	6.0	6.4	106.6	1.7
	7.0	6.7	95.7	0.7

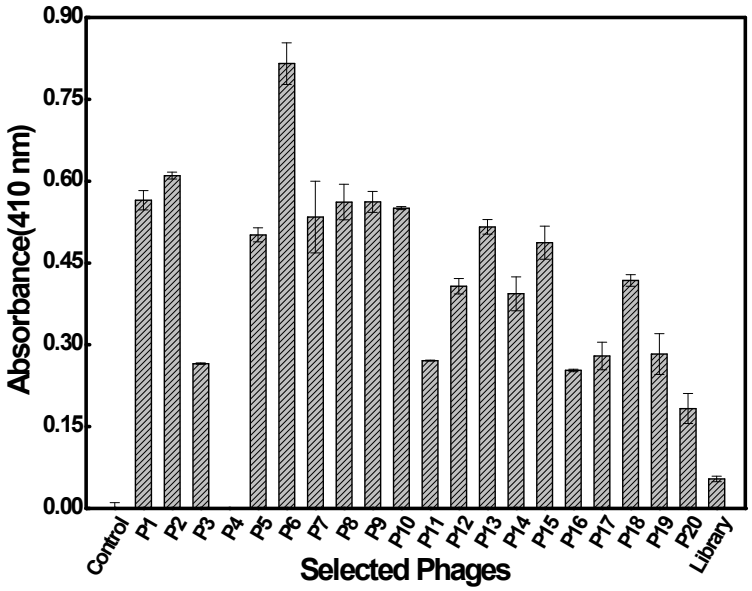

Figure S1. Binding affinity of the selected Hg^{2+}-binding phages for Hg^{2+}.

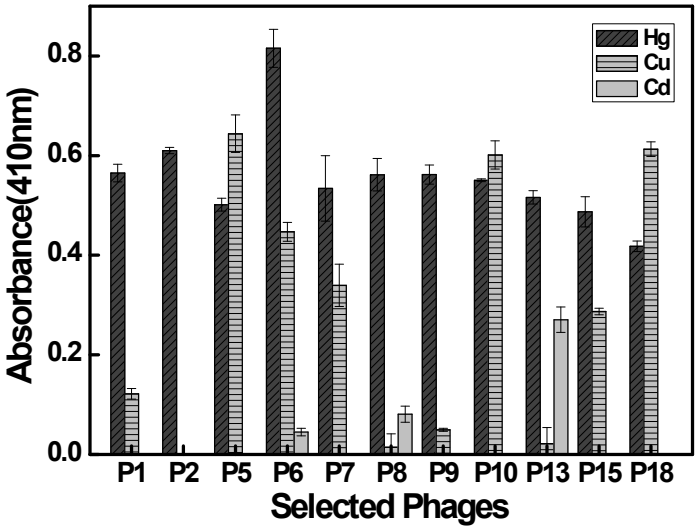

Figure S2. Binding specificity of the selected Hg^{2+}-binding phages for Hg^{2+}, $Cu^{2+}$and Cd^{2+}.

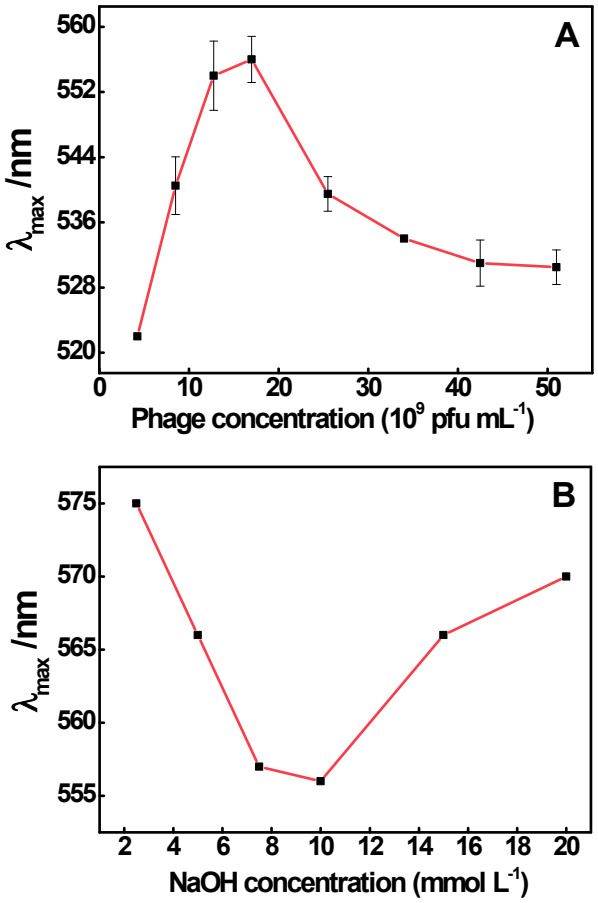

Figure S3. λ_{max} for the AuNPs-phage networks with different synthesis conditions of phage concentration (A) and solution acidity (B).

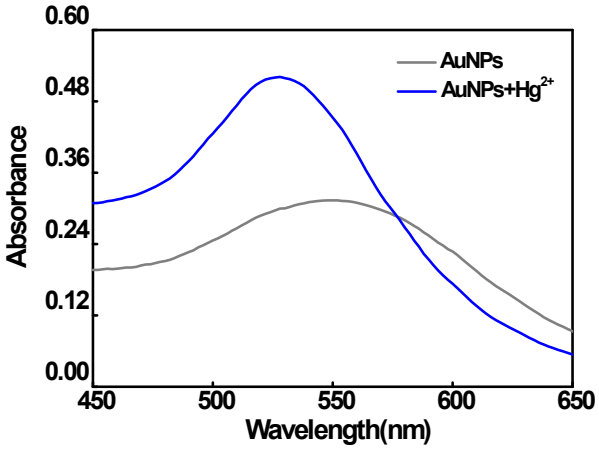

Figure S4. UV-vis absorption spectra of the AuNPs-phage networks before and after the addition of Hg^{2+}. Hg^{2+} concentration: 10 μmol L^{-1}.

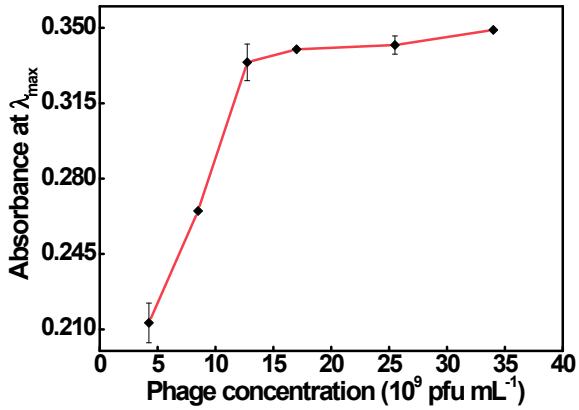

Figure S5. Absorbance at λ_{max} for the AuNPs-phage networks as a function of the phage concentration.

As can be seen in Figure S5, the absorbance at λ_{max} for the AuNPs-phage networks was almost unchanged when the phage concentration is higher than 1.7×10^{10} pfu mL^{-1}, indicating that a final phage concentration of 1.7×10^{10} pfu mL^{-1} is already enough to reduce 243 μmol L^{-1} of chloroauric acid, i.e., the phage is excessive with respect to $HAuCl_4$ in the present system.

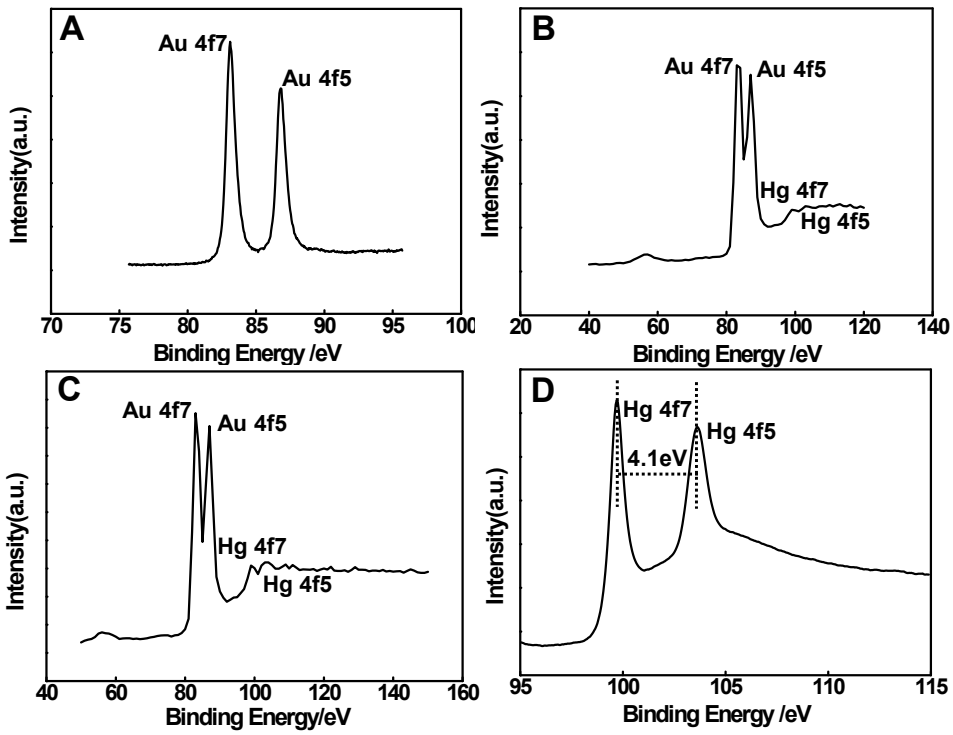

Figure S6. XPS spectra of AuNPs in the absence of Hg^{2+} (A); and XPS spectra in the presence of Hg^{2+} (B: 30 μmol L^{-1}; C and D: 50 μmol L^{-1}).

For XPS measurements, samples were centrifuged and freeze dried. All the core level binding energies (BE) were corrected according to the C1s BE at 284.8 eV.

AuNPs: The Au 4f peak in the control sample could be decomposed into two chemically distinct peaks at 87 and 83.3 eV, which correspond to Au(0)[24] (Figure S6A). The absence of a peak at 84.9 eV corresponding to Au (III) confirmed the gold atoms are present as Au (0).

AuNPs +30 μmol L^{-1} Hg^{2+}: The position of the high intensity Hg 4f peaks were found to be at 99.05 and 103.15 eV that corresponds to the Hg (0) oxidation state, which confirmed that elemental mercury was formed by reduction. The absence of two peaks at 69.3 eV for 5p1 and 74.35 eV for 5p3 suggested the absence of Hg(II)[25]. And the absence of a peak at 101.4 eV indicated the absence of Hg(I). The spectra of Au 4f can be deconvoluted into two components that correspond to the binding

energies at 86.95 and 83.2 eV suggesting the Au(0) oxidation state (Figure S6B).

AuNPs +50 µmol L^{-1} Hg^{2+}: The core-level spectrum of the Au4f region shows two peaks at binding energy values of 87.4 and 83.7 for 4f5 and 4f7, suggesting the presence of Au(0) in the sample (Figure S6C). The core-level spectrum of the Hg 4f region shows two peaks at the binding energy values of 99.05 and 103.15eV for 4f7 and 4f5, which indicate the presence of Hg in the Hg(0) state due to the formation of Au-Hg alloy upon the addition of Hg^{2+} into the AuNPs-phage networks solution. The position and binding energy difference between the two peaks is found to be 4.1 eV (Figure S6D), which matches the reported value for elemental mercury (Hg(0))[26]. The XPS survey spectra of Hg 5p region (Figure S6C) shows the absence of peaks at 69.3 and 74.35 eV for Hg5p1 and Hg5p3 indicating the absence of Hg(II) ions as well. All of the above have proved the formation of Au-Hg alloy.

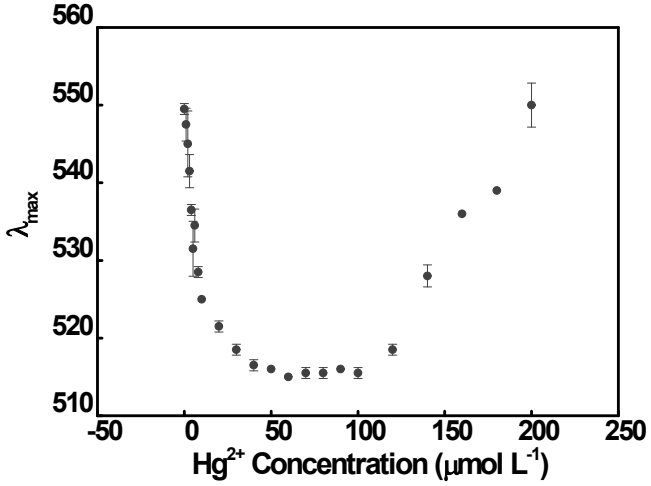

Figure S7. The SPR band (λ_{max}) of AuNPs after the addition of Hg^{2+} of various concentrations.

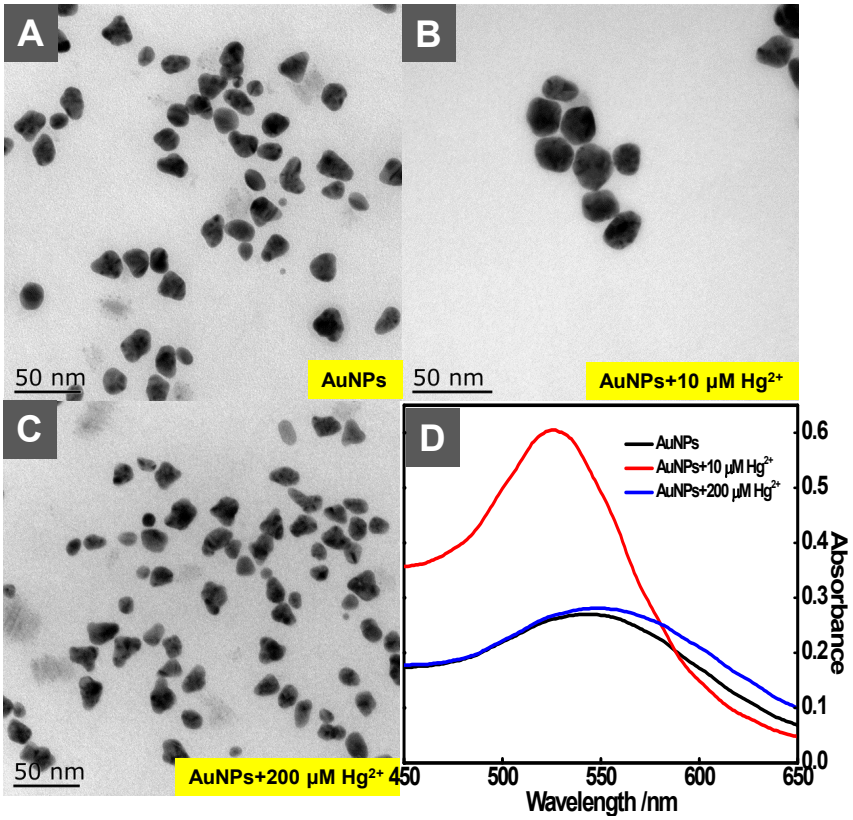

Figure S8. TEM images of AuNPs before (A) and after the addition of 10 μmol L^{-1} (B) and 200 μmol L^{-1} of Hg^{2+}(C) and the corresponding UV-vis absorption spectra (D).

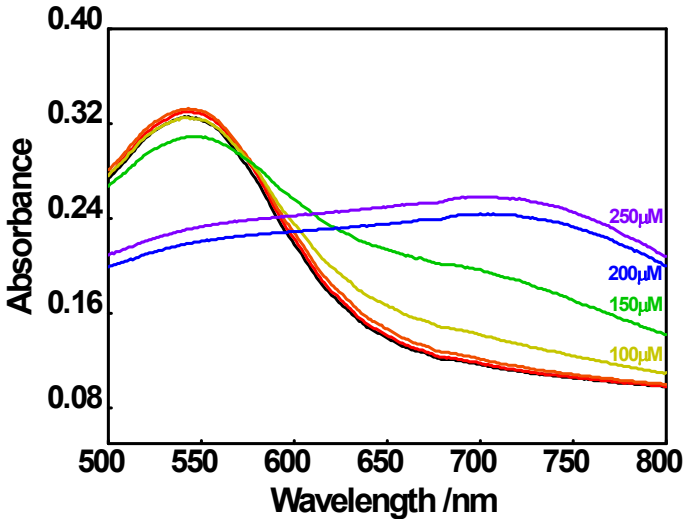

Figure S9. UV-vis absorption spectra of AuNPs with excessive phages removed upon the addition of Hg^{2+}.

The AuNPs-phage networks were first repeatedly centrifuged (1,5000 rpm, 15 min, 3 times) and washed to remove the excessive phages. The remaining AuNPs were re-suspended in DI water with the acidity and concentration adjusted to the same as the AuNPs-phage networks. Different concentrations of Hg^{2+} (0, 10, 50, 100, 150, 200 and 250 μmol L^{-1}) were added in the re-suspended AuNPs solutions in a volume ratio of 1:4. UV-vis absorption spectra were recorded after 40 min. As can be seen in Figure S9, the SPR band of AuNPs showed a redshift and the response was far less than that achieved by the AuNPs-phage networks.

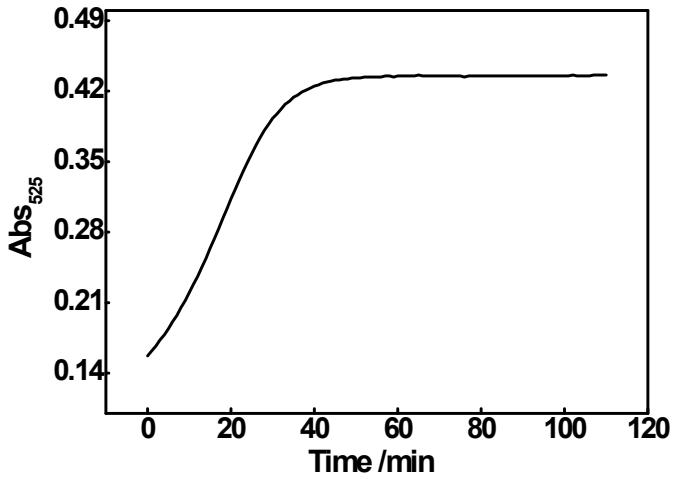

Figure S10. UV-vis absorption spectra of the AuNPs-phage networks upon the addition of Hg^{2+} as a function of time.

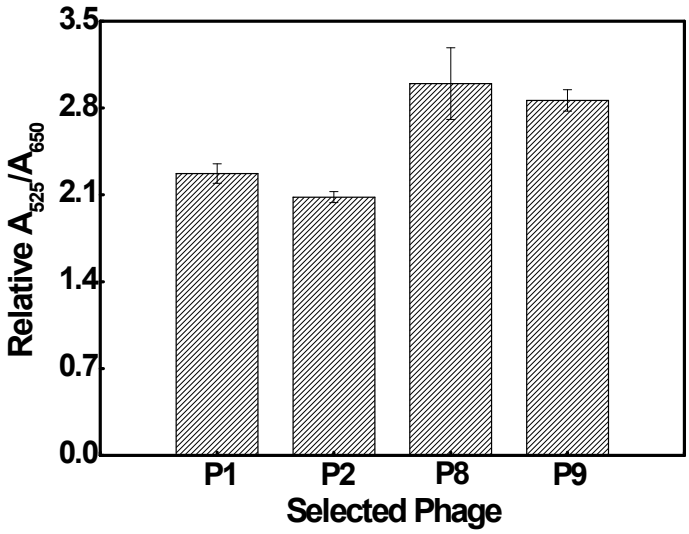

Figure S11. UV-vis absorption response to Hg^{2+} of the AuNPs-phage networks prepared with 4 kinds of the selected Hg^{2+}-binding phages.

Relative A_{525}/A_{650} means the absorbance ratio of experimental to control group.

As shown in Figure S10, the AuNPs-phage networks prepared with phage P8 give rise to the highest response. However, further comparison between phage P8 and phage P9 revealed that sensing system based on phage P9 provide a better LOD and precision, thus phage P9 was chosen for further studies.

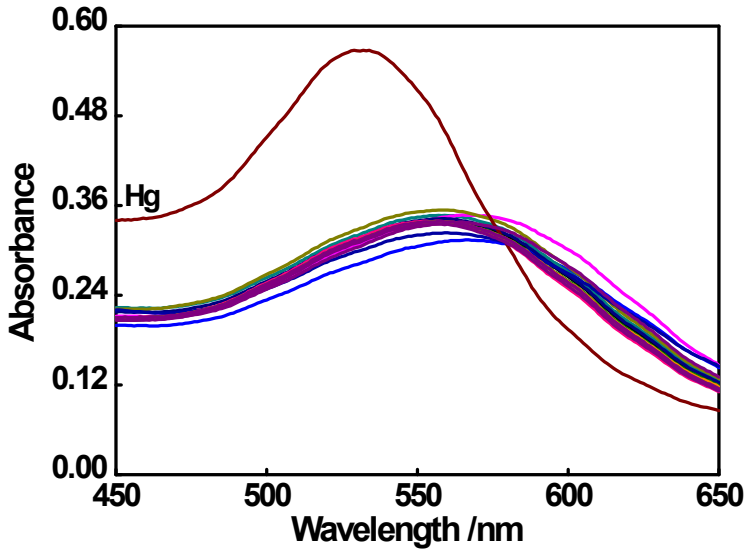

Figure S12. UV-vis absorption spectra of the AuNPs-phage networks with the addition of different metal cations. Hg^{2+}: 5 μmol L^{-1}, Ag^{+}: 10 μmol L^{-1}, other metal cations: 50 μmol L^{-1}

UV-vis absorption spectra of the AuNPs-phage networks before and after the addition of other foreign metal cations including K^{+}, Na^{+}, Ca^{2+}, Mg^{2+}, Cd^{2+}, Co^{2+}, Cr^{3+}, Cu^{2+}, Fe^{3+}, Mn^{2+}, Ni^{2+}, Zn^{2+}, Al^{3+}, and Ag^{+} almost overlap, thus was not particularly labeled in the figure.

Reference

[1] S. Si, A. Kotal, T. K. Mandal, *J. Phy. Chem. C* **2007**, *111*, 1248-1255.

[2] C.-W. Liu, Y.-T. Hsieh, C.-C. Huang, Z.-H. Lin, H.-T. Chang, *Chem. Comm.* **2008**, 2242-2244.

[3] C. J. Yu, W. L. Tseng, *Langmuir* **2008**, *24*, 12717-12722.

[4] D. Li, A. Wieckowska, I. Willner, *Angew Chem Int Ed Engl* **2008**, *47*, 3927-3931.

[5] L. Li, B. Li, Y. Qi, Y. Jin, *Anal Bioanal Chem* **2009**, *393*, 2051-2057.

[6] F. Chai, C. Wang, T. Wang, Z. Ma, Z. Su, *Nanotechnology* **2010**, *21*, 025501.

[7] Y.-R. Kim, R. K. Mahajan, J. S. Kim, H. Kim, *ACS Appl. Mater. Interfaces* **2010**, *2*, 292-295.

[8] C.-Y. Lin, C.-J. Yu, Y.-H. Lin, W.-L. Tseng, *Anal. Chem.* **2010**, *82*, 6830-6837.

[9] D. B. Liu, W. S. Qu, W. W. Chen, W. Zhang, Z. Wang, X. Y. Jiang, *Anal. Chem.* **2010**, *82*, 9606-9610.

[10] X. Chen, Y. Zu, H. Xie, A. M. Kemas, Z. Gao, *Analyst* **2011**, *136*, 1690-1696.

[11] D. Xu, H. W. Zhao, C. Z. Huang, L. P. Wu, W. D. Pu, J. J. Zheng, Y. Zuo, *J. Nanosci. Nanotechnol.* **2012**, *12*, 3006-3010.

[12] L. Chen, J. Li, L. Chen, *ACS Appl Mater Interfaces* **2014**, *6*, 15897-15904.

[13] Q. S. Wei, R. Nagi, K. Sadeghi, S. Feng, E. Yan, S. J. Ki, R. Caire, D. Tseng, A. Ozcan, *ACS Nano.* **2014**, *8*, 1121-1129.

[14] G. H. Chen, W. Y. Chen, Y. C. Yen, C. W. Wang, H. T. Chang, C. F. Chen, *Anal. Chem.* **2014**, *86*, 6843-6849.

[15] H. Chen, W. Hu, C. M. Li, *Sens. Actuators B: Chem.* **2015**, *215*, 421-427.

[16] Z. Chen, C. Zhang, H. Ma, T. Zhou, B. Jiang, M. Chen, X. Chen, *Talanta* **2015**, *134*, 603-606.

[17] Y. Deng, X. Wang, F. Xue, L. Zheng, J. Liu, F. Yan, F. Xia, W. Chen, *Anal. Chim. Acta* **2015**, *868*, 45-52.

[18] V. V. Kumar, S. P. Anthony, *Sens. Actuators B-Chem.* **2016**, *225*, 413-419.

[19] A. G. Memon, X. Zhou, J. Liu, R. Wang, L. Liu, B. Yu, M. He, H. Shi, *J.*

Hazard. Mater. **2017**, *321*, 417-423.

[20] Y. Gao, X. Li, Y. Li, T. Li, Y. Zhao, A. Wu, *Chem Commun* **2014**, *50*, 6447-6450.

[21] J. Duan, M. Yang, Y. Lai, J. Yuan, J. Zhan, *Anal Chim Acta* **2012**, *723*, 88-93.

[22] X. Xu, J. Wang, K. Jiao, X. Yang, *Biosens. Bioelectron.* **2009**, *24*, 3153-3158.

[23] C. C. Huang, H. T. Chang, *Chem Commun* **2007**, 1215-1217.

[24] N. Vasimalai, S. A. John, *J. Mater. Chem. A* **2013**, *1*, 4475.

[25] B. V. Christ, *Hand Books of Monochromatic XPS Spectra, Vol. II*, XPS international LIC, **2006**.

[26] S. Jayabal, R. Sathiyamurthi, R. Ramaraj, *J. Mater. Chem. A* **2014**, *2*, 8918. C. D. Wagner, W. M. Riggs, L. E. Davis, J. F. Moulder, G. E. Muilenberg, *Handbook of X-ray photoemission Spectroscopy*, Perkin Elmer Corp. Publishers, Eden Prairie, **1979**.